A Kernel-Based Predictive Model of EV Capacity for Distributed Voltage Control and Demand Response

Hamed Valizadeh Haghi, *Member, IEEE*, and Zhihua Qu, *Fellow, IEEE*

***Abstract*—Energy storage and reactive power supplied by electric vehicles (EVs) through vehicle-to-grid (V2G) operation can be coordinated to provide voltage support, thus reducing the need of grid reinforcement and active power curtailment. Optimization and control approaches for V2G-enabled reactive power control should be robust to variations and offer a certain level of optimality by combining real-time control with an hours-ahead scheduling scheme. This paper introduces an optimization and control framework that can be used for charging batteries and managing available storage while using the remaining capacity of the chargers to generate reactive power and cooperatively perform voltage control. Stochastic distributed optimization of reactive power is realized by integrating a robust distributed sub-gradient method with conditional ensemble predictions of V2G capacity. Hence, the proposed solutions can meet system operational requirements for the upcoming hours by enabling instantaneous cooperation among distributed EVs.**

***Index Terms*—Coordinated voltage control, distributed optimization, electric vehicles, reactive power, stochastic process.**

I. Introduction

AS UNSCHEDULED residential loads, electric vehicles (EV) might eventually induce operational complications, whereas, properly controlled charging could help improve the capacity factors of wind and photovoltaic generators [2]–[5] and supply reactive power [1], [6]–[8]. Typical mechanisms to provide demand response and reactive power services rely on the vehicle-to-grid (V2G) operation and charging strategies through either charging stations equipped with local energy storage units [9], [10], or individual charging control [11], [12].

Manuscript received November 25, 2015; revised May 7, 2016 and September 8, 2016; accepted November 4, 2016. Date of publication November 14, 2016; date of current version June 19, 2018. This work was supported in part by the U.S. National Science Foundation under Grant ECCS-1308928, by the U.S. Department of Energy Award DE-EE0006340 and Award DE-EE0007327, by the U.S. Department of Transportation Grant DTRT13-G-UTC51, by the L-3 Communication Contract 11013I2034, by Leidos Contract P010161530, and by Texas Instruments Awards. A preliminary version of this paper was presented at the American Control Conference, Chicago, IL, 2015 [1]. Paper no. TSG-01497-2015.

H. Valizadeh Haghi was with the University of Central Florida, Orlando, FL 32816 USA. He is currently with Northwestern University, Evanston, IL 60208 USA (e-mail: valizadeh@ieee.org).

Z. Qu is with the University of Central Florida, Orlando, FL 32816 USA (e-mail: qu@ucf.edu).

Color versions of one or more of the figures in this paper are available online at http://ieeexplore.ieee.org.

Digital Object Identifier 10.1109/TSG.2016.2628367

The V2G operation can be defined as the provision of energy and ancillary services from EVs to the grid [13]. The EVs can respond quickly to reactive power regulation signals. This regulation can be controlled independently by each EV charging setup in a cooperative manner. A voltage control can be embedded in the battery charger. Available ac–dc topologies to be used for reactive power support using chargers have been studied [14]. An increase in dc-link capacitor size is required and depends on the selected topology. Full-bridge converter topology requires the least increase in size compared to half-bridge, for example. Meanwhile, it can be used to compensate reactive power during both the charging and discharging of the EV batteries. A vehicle can provide reactive power irrespective of the battery state of charge (SOC). Furthermore, reactive power control and unidirectional V2G do not degrade the battery and therefore preserve its lifetime [11].

A charger can compensate inductive or capacitive reactive power by properly selecting the current phase angle. The controller meets the required charging command (P_{ref}) and the utility can control P_{ref} to coordinate charging power during the peak hours. The requested reactive power, Q_{ref} (with $Q_{ref} \leq \bar{Q}_{ref}$) as well as P_{ref} must be processed before being sent to the charger. Fig. 1 shows the components of this mechanism. The operation strategy block includes policies and requirements of the utility/operator as it can provide a controlled exchange with the main grid. It can also communicate with the rest of the network. On the other hand, in addition to the transfer of control signals (shown by arrows), this structure should provide communication among EVs and storage units. Fig. 1(b) illustrates operating regions of a full-bridge converter topology which, as explained earlier, is the best choice in charging stations.

The application of the cooperative distributed optimization to optimally dispatch the reactive power generation of DGs in a microgrid has been investigated [15], [16]. The sub-gradient algorithms as decentralized network optimization algorithms are applied to minimize a sum of objective functions (that represents the optimal voltage profile) when each component function is known only to particular agents of a distributed network [15]–[18]. However, optimization algorithms for reactive power utilization from V2G should take account of variations across time and availability of electric vehicles. Hence, a more suitable optimization algorithm for V2G-enabled reactive power control should be robust to variations and offer a certain

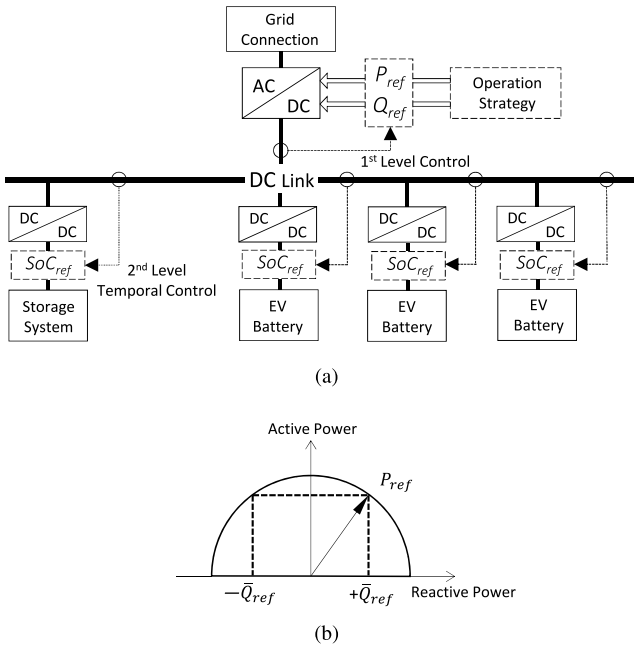

Fig. 1. (a) Control parameters of grid-connected storage for the charging station setup. (b) Operating regions for reactive power compensation subject to active power constraints.

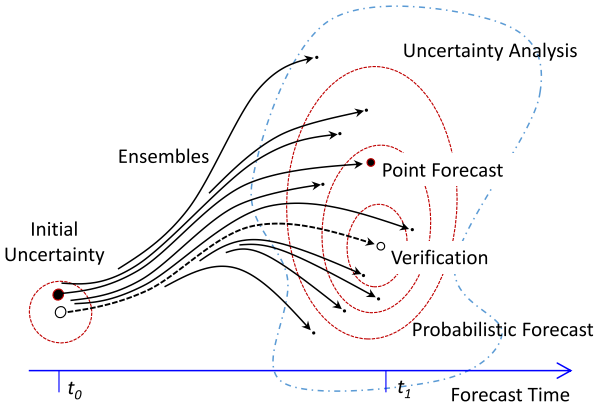

Fig. 2. Predictive inference using ensembles. The calculated ensembles can be used to build other stochastic measures of uncertainty such as density forecasts.

level of optimality by combining it with several-hours-ahead network management schemes.

The objective is to schedule charging and to enable demand response while using the remaining capacity of V2G to generate reactive power and cooperatively perform voltage control. In this paper, a robust distributed sub-gradient optimization is proposed in order to perform active power and voltage control. The implemented optimization and control consist of two approaches: (1) temporal charging control and demand response, and (2) real-time cooperative voltage/power control among DGs and EV charging stations. A kernel-based predictive modeling of available capacity from charging stations is proposed. The model is used to formulate predictive capacity allocation and demand response based on the exact probabilities associated with different resource levels. Then, a real-time cooperative distributed control is applied in order to optimally dispatch the reactive power capacity and realize a unified voltage profile while maintaining active power controls such as desired states of charge and DG constraints.

II. Multivariate Approach to Calculating Conditional Ensembles of V2G

A. Introduction

The deployment of EVs connecting to distribution networks can lead to an increased power demand and less responsive voltage profiles [19]–[21]. On the other hand, battery energy storage with V2G technology [22] is effective in buffering active and reactive power fluctuations, thus providing voltage and frequency control [23]. Hence, V2G capacity should be considered in the optimization and control procedures. Forecasts of V2G capacity are the average availability of vehicles expected to be available from the clusters of EV chargers during the considered look-ahead time. This is the so-called point forecast that provides only a single value for the considered time resolution. Extensive research has been reported on point forecasting methods which use different types of regression models (e.g., neural networks) and Monte Carlo simulation [24].

Contrary to the single-valued forecasts which only provide projected mean values of the V2G capacity, ensemble predictions can offer distributions of V2G capacity for different look-ahead times. The ability to predict exact probabilities associated with different V2G power levels in future is critical for a successful integration and control of the EV charging stations. This is particularly useful when a certain degree of robustness is ensured for the reliable operation of power system against uncertainty of point forecasts.

Ensemble predictions may refer to a wide range of methods that study different models for characterization or estimation of uncertainty. The uncertainty is reflected either in the point forecasts or in the data variations itself. Fig. 2 shows the concept of prediction ensembles: A set of quantiles represents the empirical cumulative distribution function (ecdf) that can be calculated from a full pdf by using kernel smoothing. This pdf estimates the true underlying error distribution in power forecasting and can be provided by either a parametric or a non-parametric representation. Non-parametric or empirical representation is the most natural and accurate way of modeling the ensembles; because it can reflect on how the real EVs behave and error data changes and can be calculated from historical data [25].

On the other hand, most probabilistic forecasts are provided for consecutive look-ahead times independently. Hence, they lack any information on the characteristics that drive the temporal evolution of V2G capacity and error data. In fact, the cross-correlations and dependencies between the forecasting error series over the considered time horizon are valuable characteristics, particularly, for power system problems that have time-dependent memory such as in energy storage management. Also, most of the available methods cannot satisfactorily cope with non-Gaussian data typical in power systems.

In this section, a spatio-temporal multivariate modeling for calculating ensembles of V2G capacity is proposed. This provides a considerable extension over the previous work

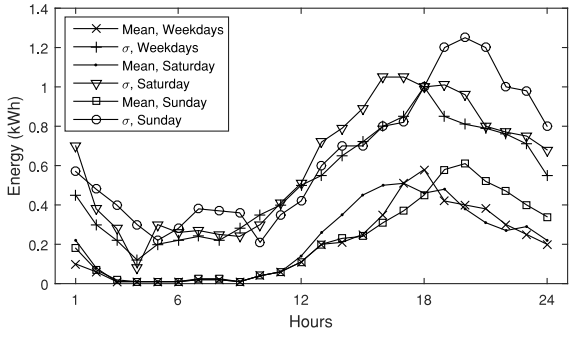

Fig. 3. Mean and standard deviations for the capacity available from EVs with 10 kW charging power on workdays and holidays [25].

presented in [14]. The main goal is to capture the temporal dependence of V2G capacity conditional on distributions of forecast error at each look-ahead time. The proposed algorithm uses copula-based modeling. Once the model is fitted to the historical data, the conditional ensembles can be calculated very fast. This can be viewed as an adaptive probabilistic forecasting for several-hours look-ahead time periods. Historical EV data from [25] is used to build the model.

B. Proposed Modeling for Predictive Inference

Ensemble predictions can be used in predictive inference procedures in order to deal with the uncertainty of point forecasts [26]. Future outcomes of V2G capacity, according to the estimated probability, will fall in between ensembles, given what has already been observed. The main objective is to provide an empirical distribution of error for a current expected value; hence, the inherent uncertainty of point forecasts can be predicted.

The first step is to convert the raw driving data into the charging profiles. This is done by tracking the trips of the cars and calculating the SOC and charging power of the batteries. Then, the hourly charged energies of the cars can be calculated based on the individual charging events. It should be noted that the main parameters to be considered are the battery capacities, power requirements of the EVs, charging station capacity, and customer classification.

The second step, as described in this section, is to build a predictive model that fits the converted data. A multivariable modeling structure is proposed that is used for calculating predictive ensembles of the available V2G capacity. The main modeling parameter is the active power profiles at the charging stations. The capacity of the chargers to support reactive power can then be calculated considering the number of chargers in use as well as the chargers available for reactive power support only. The data from [25] is used as historical information to build the conditional ensembles. Mean and standard deviation of a sample set of Finland's data are shown in Fig. 3, as repeated from [25]. Once the historical charging profiles is calculated from the raw data, the proposed modeling can be built. The modeling concept is as follows.

Assume a one-dimensional function $g(t) = P_i(t)$ that represents capacity of the i^{th} V2G charging station with a set of noisy observations $\mathbf{p}_i = \{p_i(t_j)\}_{j=1}^{N} = g(\mathbf{t}) + \varepsilon_n$ at $\mathbf{t} = \{t_0 + jT\}_{j=1}^{N}$, where, T is the time step. Distribution of ε_n which is mainly due to the measurement errors is represented in the covariance matrix and discussed toward the end of this section. In order to predict values of this function, $\mathbf{p}_i^* = \{p_i^*(t_k)\}_{k=1}^{M}$, at $\mathbf{t}^* = \{t_0^* + kT\}_{k=1}^{M}$, the joint distribution of the observed and predicted values can be constructed as follows:

$$\begin{aligned}\Pr\left(\mathbf{P}_i \le \mathbf{p}_i, \mathbf{P}_i^* \le \mathbf{p}_i^* \middle| \mathbf{t}, \mathbf{t}^*\right) &= C\left(\left\{F_j\left(p_i(t_j)\right)\right\}_{j=1}^{N}, \left\{F_k\left(p_i(t_k)^*\right)\right\}_{k=1}^{M} | \mathbf{t}, \mathbf{t}^*\right) \quad (1)\\ &= C\left(\left\{u_j\right\}_{j=1}^{N}, \left\{u_k^*\right\}_{k=1}^{M} | \mathbf{t}, \mathbf{t}^*\right) \quad (2)\end{aligned}$$

where, $C(.)$ is the copula function [27], [30], $F_j(p_i(t_j))$ is the marginal cumulative distribution functions (cdfs) of the V2G capacity and u_j is the transformed $p_i(t_j)$ via $u_j \doteq F_j(p_i(t_j))$. The multivariate distribution of can be calculated by differentiation:

$$\begin{aligned}\Pr\left(\mathbf{p}_i, \mathbf{P}_i^* \middle| \mathbf{t}, \mathbf{t}^*\right) &= c\left(\left\{F_j\left(p_i(t_j)\right)\right\}_{j=1}^{N}, \left\{F_k\left(p_i(t_k)^*\right)\right\}_{k=1}^{M} | \mathbf{t}, \mathbf{t}^*\right)\\ &\times \prod_{j=1}^{N} f_j\left(p_i(t_j)\right) \prod_{k=1}^{M} f_k\left(p_i(t_k)^*\right) \quad (3)\end{aligned}$$

where, $f_j(p_i(t_j))$ is the marginal pdfs and $c_i(.)$ is the copula density which is obtained by the derivative of the coupla function:

$$c\left(\left\{u_j\right\}_{j=1}^{N}\right) = \frac{\partial^N C}{\partial u_1 \partial u_2 \cdots \partial u_N} \quad (4)$$

This formulation offers a unified multivariate model of the prediction data that includes exact nonlinear dependence structure subsequently required to estimate ensembles. The fundamental definition of copula functions is out of the scope of this short paper; however, a copula function can be simply defined as the joint distribution of two or more random vectors each transformed as uniform random variables. Advantages of using copulas for multivariate data are considerable. First, by using copula modeling concept, the joint distribution can be decomposed into the dependency structure (copula function) and the marginal distributions. Hence, each variable can be described by a different distribution (e.g., Gaussian, Weibull, or even empirical distributions). Furthermore, copula functions capture the complete dependence structure that is unlike the linear correlation coefficient which only measures co-variations up to the second order [30].

In summary, the structure of the proposed model is composed of three elements,

1) copula function,
2) kernel function, and
3) marginal distributions.

As mentioned above, the copula function as the main part of the model enables accurate and efficient construction of the dependence structure between variables. One of the benefits is the ability to model high-dimensional and long-range data sets. On the other hand, the kernel function helps to achieve predictive performance which is illustrated in the following section. The third element, the marginal distributions, provide enough flexibility to match the observed process, especially in the applications where the data is non-Gaussian. This is

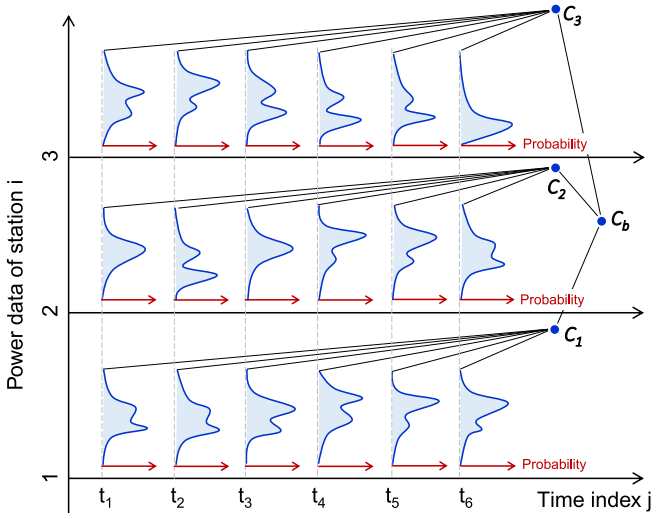

Fig. 4. An illustration of the model's structure for three charging stations.

possible thanks to the copula modeling concept following the Sklar's theorem [27].

The proposed model can then be extended to multivariate time series when there are multiple aggregators and charging stations, or even load or solar power data to be considered. One option is to parameterize (1) using an additional copula function C_b:

$$\begin{aligned}\Pr\left(\mathbf{P}_1 \le \mathbf{p}_1, \ldots, \mathbf{P}_\eta \le \mathbf{p}_\eta\right) &= C_b\Big[C_1\left(\left\{F_j\left(p_1(t_j)\right)\right\}_{j=1}^{N_1}\right) \\ &\quad \times \cdots \times C_\eta\left(\left\{F_j\left(p_\eta(t_j)\right)\right\}_{j=1}^{N_\eta}\right)\Big] \end{aligned} \tag{5}$$

The related proof and analyses behind 5 is provided in the Appendix. Fig. 4 shows the graphical structure of the model. This schematic illustrates how the additional copula joins multiple time-based station's data together. The advantage of this model is that data with from different resources and specific characteristics can be modeled.

Model calculations can be carried out by maximizing likelihood. A general likelihood function for the univariate model, (3), is given by:

$$\begin{aligned}\ell_i(\lambda) &= \Pr(\mathbf{p}_i|\mathbf{t}, \lambda) \\ &= c\left(\left\{F_j\left(p_i(t_j)\right)\right\}_{j=1}^{N}\right)\prod_{j=1}^{N} f_j\left(p_i(t_j)\right)\end{aligned} \tag{6}$$

where, $\mathbf{p}_i$ is the set of historical data for the i^{th} station or source and λ is the set of parameters for the copula functions. The likelihood for the multivariate model, (5), can be derived from (6):

$$\begin{aligned}\ell(\lambda) &= \Pr\left(\mathbf{p}_1, \ldots, \mathbf{p}_\eta\right) \\ &= \frac{\partial^\eta C_b}{\partial C_1 \cdots \partial C_\eta} \times \left(\frac{\partial^{N_1} C_1}{\partial u_1(p_1) \cdots \partial u_{N_1}(p_1)} \prod_{j=1}^{N_1} f_j\left(p_1(t_j)\right)\right) \\ &\quad \times \cdots \times \left(\frac{\partial^{N_\eta} C_\eta}{\partial u_1\left(p_\eta\right) \cdots \partial u_{N_\eta}\left(p_\eta\right)} \prod_{j=1}^{N_\eta} f_j\left(p_\eta(t_j)\right)\right) \\ &\doteq c_b \times \ell_1(\lambda_1) \times \cdots \times \ell_\eta\left(\lambda_\eta\right)\end{aligned} \tag{7}$$

where, the partial derivatives with respect to the cdfs follow (4)'s notation. It is important to note that (7) enables a modular structure to learn all of the model parameters either at the same time, or separately.

III. Model-Based Conditional Ensembles

One of the benefits of the proposed modeling structure is that the complete predictive distribution (illustrated in Fig. 2) is available for inference, hence, allowing for constructing ensembles by regular sampling techniques. The predictive distribution of the proposed model in the previous section can be calculated by:

$$\Pr\left(\mathbf{p}_i^*|\mathbf{p}_i\right) = \frac{C_{\widehat{\Psi}}\left(\left\{F_j\left(p_i(t_j)\right)\right\}_{j=1}^{N}, \left\{F_k\left(p_i^*(t_k)\right)\right\}_{k=1}^{M}\right)}{C_\Psi\left(\left\{F_j\left(p_i(t_j)\right)\right\}_{j=1}^{N}\right)} \tag{8}$$

where, Ψ is calculated from the observations and $\widehat{\Psi}$ is derived from both observations and targets data of V2G capacity according to the following covariance matrix:

$$\Psi = \begin{bmatrix} \psi(t_1, t_1) & \cdots & \psi(t_1, t_N) \\ \vdots & \ddots & \vdots \\ \psi(t_N, t_1) & \cdots & \psi(t_N, t_N) \end{bmatrix} + \sigma_n^2 \mathbf{I} \tag{9}$$

where, $\psi(t_j, t_k)$ is a kernel function of the covariance between pairs of $p_i(t_j)$ and $p_i(t_k)$, and σ_n^2 is the noise variance and $\mathbf{I}$ is the identity matrix. A small noise variance is assumed in this paper that follows a standard Gaussian distribution. Nonetheless, verifying that the noise is negligible or Gaussian should be done on a case-by-case analysis for different applications and data sources. Here, the radial basis function is used as a kernel as it provided the best fit to the data:

$$\psi\left(t_j, t_k\right) = \exp\left(-\frac{\left(t_j - t_k\right)^2}{2\sigma^2}\right) \tag{10}$$

where, σ is a free parameter that sets the *spread* of the kernel. Numerical calculations are also useful once the multivariate model is calculated. First, a comprehensive look-up table that includes a large number of samples should be constructed by sampling from the model of forecasting/projection data. Then, the conditional pdf of interest is calculated simply by searching for the realized patterns of V2G capacity and projection errors over the forecasting interval N using the look-up table. This simple procedure is justified based on the following:

$$\begin{aligned}f(u_1, u_2, \ldots, u_n) &= f_1(u_1) f_2(u_2|u_1) \times \cdots \\ &\quad \times f_n\left(u_n^*|u_1, \ldots, u_{n-1}\right)\end{aligned} \tag{11}$$

where, $f_n(u_n^*|u_1, \ldots, u_{n-1})$, as the only parameter to be determined, represents conditional error distribution of the ensemble of interest given that $U_1 = u_1, \ldots, U_{n-1} = u_{n-1}$.

Fig. 5 summarizes the proposed method in a detailed flowchart. The flowchart illustrates how the ensembles (equivalently, scenarios or data samples) can be calculated. Ensembles predict future variations in the charging stations' capacity and

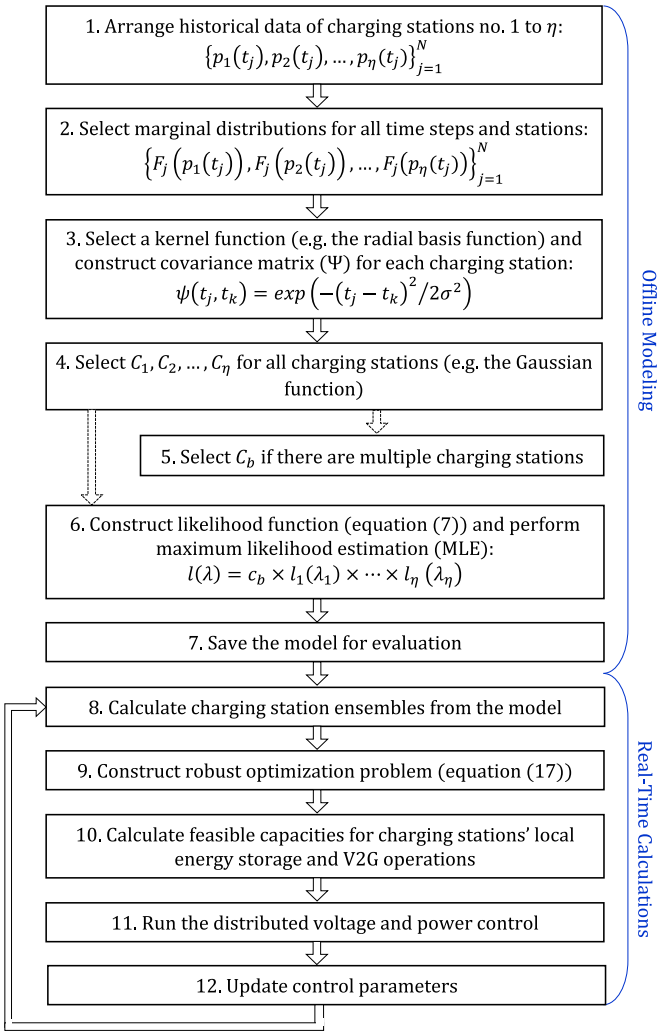

Fig. 5. Stages of the proposed method: offline modeling and real-time calculation and robust optimization.

are used as inputs to the optimization problem. They should exploit critical characteristics leading to a robust decision policy. The optimization stages are described in the following section. Practical benefits of the proposed predictive approach for voltage control and demand response are also studied in the same section. It should be noted that the modeling and most of the required calculations can be handled off-line. Hence, real-time or on-line operations would be more efficient.

Sample computational times are given in the final case study. It should be noted that the whole procedure is targeted for real-time applications with fast computational times in order of seconds to minutes depending on the setup. The modeling calculations, on the other hand, can be done off-line and undergo updates at regular time intervals (e.g., seasonal or monthly updates) to account for major changes in customer behavior and/or resources.

Solution algorithms are coded on MATLAB/Simulink while parts of the pseudo-codes from R [32] are used for model estimation. The modeling algorithms that follows Fig. 5 is discussed in the following subsection.

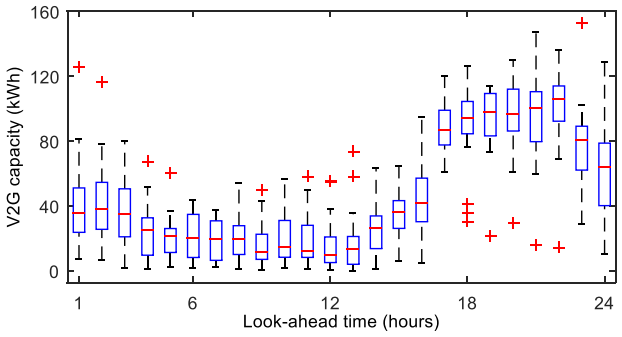

Fig. 6. Example of the calculated distribution of the ensembles along with the point projections using the proposed multivariate algorithm.

A. Solution Algorithm

Following stages are essential in implementing the predictive model:

1) Selecting marginal distribution: The proposed model is compatible with any parametric or empirical distributions. If a parametric distribution is chosen, then the associated parameters are learned with the maximum likelihood estimation (MLE).
2) Designing the kernel function: Using the auto-correlation functions (ACFs) of the first few moments of data, algorithms from [35] can be used to design kernels. In this paper, the radial basis function is used.
3) Selecting copula functions: Gaussian copula is chosen for the proposed model as it effectively represents dependencies across time which is the main interest.
4) Full model training: for a given load time-series, the MLE can be used on a sliding window over data based on the likelihood for the full model according to (7).

B. Load Modeling Results

Aforementioned solution algorithms are implemented in MATLAB and assuming a time resolution of 1 hour, modeling and prediction takes up to 15 minutes to complete on a Core i5 2.2 GHz machine. Fig. 6 shows calculated conditional ensembles using the proposed multivariate algorithm corresponding to the contribution of 100 vehicles having the capacity profiles according to Fig. 3. It should be noted that this is a box and whisker plot. A box and whisker plot is a way of graphically comparing distributions between several sets of data through their five-number summaries. On each box, the central mark is the median, the edges of the box are the 25th and 75th percentiles, the whiskers extend to the most extreme data points not considered outliers, and outliers are plotted individually by a plus sign.

In order to compare the immediate results of the proposed predictive modeling with existing models, a case study is created by the following assumptions:

1) Autoregressive integrated moving average (ARIMA) [29] and Gaussian process (GP) [34] models are used for comparison which provide established benchmarks to demonstrate the effectiveness of the proposed model.

2) The data simulation algorithm in [25] is used as the base case and to carry assumptions on the EV fleet.
3) It is assumed that the charging starts immediately when the vehicle is parked at the station which provides a neutral comparison. Smart charging can also be considered without any modification in the predictive modeling because the predictive models are built upon the stations data obtained from the calculations and measurements of the charging mechanisms or patterns.
4) Time resolution is one hour and it is assumed that the vehicles are fully charged at the beginning of the first trip.
5) Charging stations equipped with local energy storage serve the fleet size of $N = 120$ as the default local population of EVs. Number of charging ports is $M = 50$ which defines the default aggregation level.
6) The fleet is divided in three equal-sized categories with average capacities of 5 kWh, 10 kWh, and 15 kWh. Battery capacities of each sub-fleet is normally distributed with standard deviation of 0.1.

Comparison is in terms of predictive capabilities of the three models over load data and is therefore independent of the above assumptions and EV charging or handling mechanisms.

Four scores are used to quantify the outcomes of the proposed and benchmark methods. Two deterministic scores include root mean square error, RMSE $= \sqrt{1/T \sum_{t=1}^{T} (x_t - \hat{x}_t)^2}$, and mean absolute error, MAE $= 1/T \sum_{t=1}^{T} |x_t - \hat{x}_t|$, where, $\hat{x}_t$ is the predicted value of x_t. Scoring rules such as the logarithmic score and the continuous ranked probability score (CRPS) can be calculated for evaluating accuracy of the predictions [28]. The CRPS is a reliable tool for probabilistic forecast evaluations, particularly for ensemble predictions [29]. The CRPS is defined for the h-step ahead predictive density function $f_{t+h|t}$, let $F_{t+h|t}$ be the corresponding cumulative distribution function. Then, the CRPS is defined as:

$$\text{CRPS} = \int_0^1 \left[F_{t+h|t}(x) - \mathbf{1}(x - x_{t+h})\right]^2 \tag{12}$$

where, $\mathbf{1}(x - x_{t+h})$ is the indicator function which is equal to one when $(x - x_{t+h})$ is positive. The log score on the other hand, is defined as the mean negative log of the forecast density function evaluated at the corresponding observation, log score $= \frac{1}{T} \sum_{t=1}^{T} - \log(f_{t+h|t})$.

Forecast performance scores of the proposed method for the predictive ensembles of Fig. 6, calculated in percent of the rated power, averages on 4.2048 and 6.1509, respectively. These are average values using the data samples from [25] assuming 95% confidence. Calculated scores prove high accuracy of the predictive ensembles. It should be mentioned that the CRPS reduces to the mean absolute error (MAE) if the prediction is deterministic. Comparison of the performance scores of all methods for 6 hours time horizon are listed in Table I. Both probabilistic and deterministic performance scores show noticeable improvement over the benchmark methods.

TABLE I
FORECASTING PERFORMANCE OF THE METHODS (MEAN OF ENSEMBLE SKILL SCORES AS % OF RATED POWER AND 95% CONFIDENCE INTERVAL)

Category	Score	Proposed	ARIMA	GP
Weekdays	CRPS	4.8421	11.2312	9.8289
	Log Score	5.2094	12.1923	12.0215
	RMSE	7.5239	15.4980	14.9014
	MAE	5.0842	13.7815	10.2045
Saturdays	CRPS	3.9024	10.8402	9.7122
	Log Score	4.8225	12.8105	10.9142
	RMSE	7.1240	14.6209	11.5023
	MAE	4.8105	12.4908	9.2986
Sundays	CRPS	5.0184	12.5811	11.1057
	Log Score	6.0021	14.9604	14.8243
	RMSE	8.2580	14.4235	15.2816
	MAE	5.9972	14.6315	12.6687

IV. STOCHASTIC DISTRIBUTED OPTIMIZATION OF V2G CAPACITY

A. Reactive Power Optimization for Distributed Voltage Control

The conditional ensembles, developed in the previous section, are used to compensate for temporal variations of V2G capacity. The deterministic optimization basis using subgradient method is according to [15] which is used for comparison and verification. The objective is to minimize the overall network voltage deviations in order to achieve a unified voltage profile across all active nodes. This objective can be realized by controlling the reactive power capacity of every DG, ESS, or EV (as the control units) which is subject to a number of stochastic constraints. In this section, the proposed stochastic constraints based on the predictive ensembles are presented. The stochastic method is formulated as an addition to the deterministic approach and compensates for temporal control and robust optimization of reactive power and demand response. Then, the deterministic cooperative optimization is briefly explained and a modification to the deterministic optimization is applied to account for the uncertainty of the communication network.

The conditional ensembles, described in the previous section, are applied to calculate a robust feasible value for $\bar{Q}_i$, i.e., the maximum available capacity for reactive power compensation, in the course of optimization. Hence, the temporal characteristics of V2G capacity and energy storage requirements is considered in a way that using V2G capacity for reactive power generation is coordinated with upcoming requirements for active power and proper management of energy storage can be realized. Nonetheless, this is the general concept and different rules can be applied to calculate and impose a feasible and admissible $\bar{Q}_i$. These rules and settings would be based on cooperative benefits to the grid that can be set according to both economic and technical considerations. As an example, the following rule is proposed here to decide upon a suitable $\bar{Q}_i$ for each unit in real-time calculations.

The energy stored in the unit at the end of the time interval, $E_i(t_N)$, for which the ensembles are calculated, is maintained.

Also, $E_i(t) \triangleq SOC_i(t)$, defines energy content of the charging station in relation to the sate-of-the-charge. The constraints are defined for all time steps within the considered look-ahead horizon. First constraint governs active power available at each time step to compensate for different ensembles of V2G capacity:

$$P_i^{min}(t) \leq P_i(t) \leq P_i^{max}(t) \tag{13}$$

where, $P_i^{min}(t) \geq 0, \forall t$ in this study, however, negative values are possible for bidirectional V2G. Constraints on energy content over each time period are as follows:

$$0 \leq SOC_i^{min}(t) \leq SOC_i(t) \leq 1, \tag{14}$$

and,

$$SOC_i(t) \underset{t \to t_N}{\longrightarrow} SOC_i^{ref} \tag{15}$$

where, $SOC_i^{ref} = 1^-$ (near-full battery/storage status) is chosen in the case study. It should be mentioned that additional discharging is possible when an ensemble exceeds the actual availability. To tackle this issue, the lower bound in (14) considers the energy demands for the next trip that is the minimum state of charge associated with the storage (both local and onboard). Finally,

$$\sum_i P_i(t) \leq P_{total}^{max} \tag{16}$$

where, P_{total}^{max}, is the threshold load, and can be calculated based on the stochastic ensembles. Additional power is delivered through the point of common coupling (PCC).

A robust optimization can then be formed that limits real-time usage of the chargers capacity for an effective reactive power control through solving the following at each time over the control period:

$$\max \ \left\{ \min_i \ \bar{Q}_i \right\} \tag{17}$$

$$\text{s.t.} \ \ \bar{Q}_i = \sqrt{S_i^2 - P_i^2} \tag{18}$$

$$\Pr[(12) \text{ to } (15)] \geq 1 - \varepsilon, \quad \forall t \tag{19}$$

where, S_i is the nominal rating of the i^{th} charger at each time, and ε is a small probability of violation. The constraint (18) is probabilistic and might be violated with probability ε. This constraint guarantees that the probability of having an inefficient energy level in the near future remains very low (i.e., 5% in the case study) and makes sure that the V2G operation can compensate for temporal integration of generation, storage, and demand.

Now, the deterministic real-time control can be implemented using the calculated temporal solution. Assume that the DGs along with the combination of local ESS and V2G operations, cooperatively minimize the following objective function:

$$F = \sum_{i=1}^{N} f_i = \sum_{i=1}^{N} \frac{(1 - V_i)^2}{2} \tag{20}$$

where, V_i is the voltage of the unit i, and each unit exchanges information on the objective components with other units. The control/optimization variables are unit's reactive power utilization defined as the reactive power provided by V2G or DGs defined as $Q_i/\bar{Q}_i$ where, Q_i and $\bar{Q}_i$ are the generated and maximum available reactive power. The variable $\alpha_i = Q_i/\bar{Q}_i$ is an estimation provided to the unit i at time step k. Unit i receive updates based on the cooperative control law:

$$\alpha_i(k+1) = \sum_{j=1}^{N} d_{ij}\alpha_j(k) - \beta_i g_i \tag{21}$$

where, d_{ij} is calculated based on the instantaneous communication topology according to [16], β_i is one step size gain associated with unit i, and g_i is the sub-gradient of the unit i's objective component, i.e., $\frac{1}{2}(1 - V_i)^2$ with respect to α_i. The gains, β_i, should be heuristically selected to achieve best performance. The sub-gradients in (21) for the units of interest are calculated as follows:

$$g_i = \frac{-\bar{Q}_i(1 - V_i)V_i}{Q_i - V_i^2 B_{ii}} \tag{22}$$

where B_{ii} is the sum of the imaginary parts of the line conductances, connecting node to the neighboring nodes. If the reactive power capacity of a unit or a node is zero, it can utilize other units reactive power capacity, hence, participating in $\bar{Q}_i$.

The following modifications explain a randomized sub-gradient method [17], [18] that is employed in order to address the communication uncertainty among distributed units where the unit that updates is selected randomly according to a distribution, conditional on the most recent updates. This is intended to represent the spatial uncertainty or potential displacement of data exchange among units. It should be emphasized that the randomized version of the sub-gradient method is in addition to the predictive ensembles that are used to compensate for temporal effects.

Suppose at time k, the j-th charger updates and generates its estimate α_k. Then, charger j may pass this estimate to its neighboring charger and/or DG i with probability $[\rho(k)]_{i,j}$. Formally, the update rule for this method is given by

$$\alpha_i(k+1) = \Im_{\mathrm{A}}\big[\alpha_i(k) - \beta_i(k+1)(\nabla f(\alpha_i(k)) + \varepsilon(k+1))\big] \tag{23}$$

where $\alpha_0 \in \mathrm{A}$ is a random initial vector, α_k represents the main optimization variable at time step k, $\varepsilon(k+1)$ is a random noise vector and $\beta(k+1) > 0$ is the step-size gain, defined above. Also, $\Im_{\mathrm{A}}$ denotes Euclidean projection onto the set A and $\nabla f(\alpha)$ is the subgradient of f evaluated at α. The indices of unit updates in time evolves according to the sequence $\{s(k)\}$, a time non-homogeneous Markov chain with states $1, \ldots, m$. If $\rho(k)$ denotes the transition matrix of this chain at time k,

$$[\rho(k)]_{i,j} = \Pr\{s(k+1) = j | s(k) = i\}, \tag{24}$$

for all $i, j \in \{1, \ldots, m\}$. When there are no errors, i.e., $\varepsilon(k+1) = 0$, and the probabilities $[\rho(k)]_{i,j} = \frac{1}{m}$, the modified method corresponds to (21). The reactive power utilization of the i-th EV/unit is denoted by α_i.

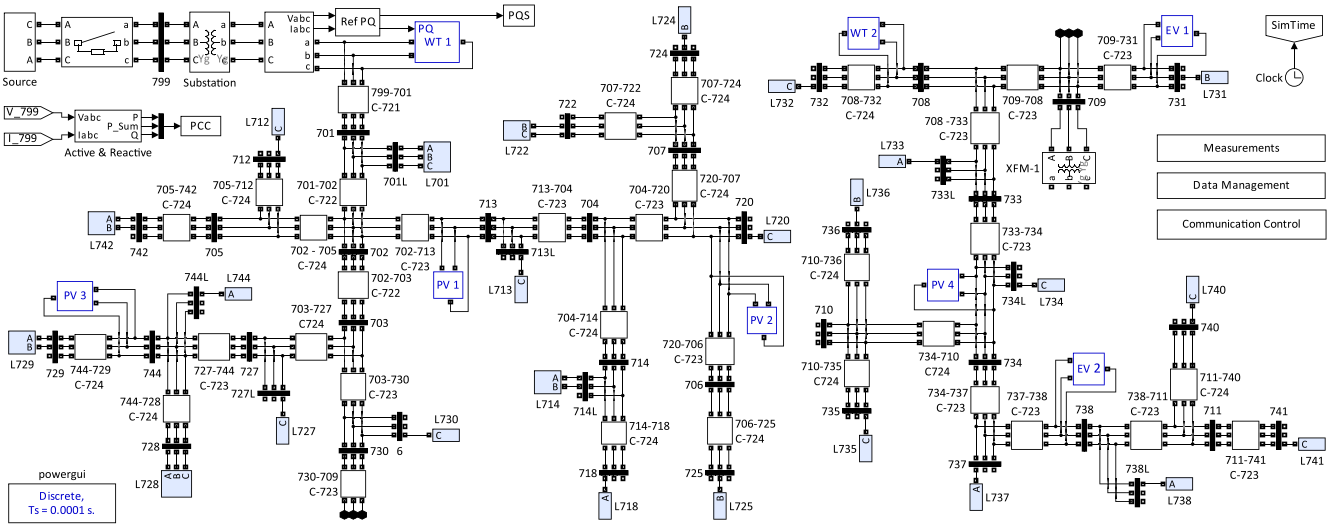

Fig. 7. IEEE 37 node test feeder with DG and EV stations locations.

B. Case Study: Utilizing V2G Capacity Within a Wind-PV-Based Microgrid

A modified version of test network by the IEEE 37 node test feeder [31] is used in the case study. This feeder is chosen as it resembles an actual feeder in California with noticeable voltage drop and unbalance for a network at this scale. All regulators and reactive power compensation devices are removed from the text feeder in order to demonstrate effective operation of the proposed controls. Spot loads and line data are according to [31] with the same configuration codes assigned to each line (e.g., C-721). The simulated feeder with all subsystems and controls in MATLAB-Simulink is shown in Fig. 7. Distributed control and robust optimization are coded using S-Functions and Simulink toolboxes all within MATLAB. Each subsystem box includes required controls, communication, data models and power sources to implement distributed active and reactive power operations. The real-time calculations and predictive robust adjustments take less than 1 second on a Core i5 2.2 GHz PC which is more than sufficient for the voltage control and demand response.

In the deterministic distributed optimization, PVs 2 and 3 minimize the aggregated reactive power flow to the main grid. All other DGs and EV charger aggregations participate in the distributed optimization in order to minimize the sum of the voltage deviations for the corresponding nodes. The gradient gains are $\beta_i = 15$ for all the DGs and EV stations. Maximum capacity of DGs are 1.2 MW for wind generation units, and 1 MW for PV units. On the other hand, EV charging stations operate within 1.5 MW range.

Simulations are carried out using the MATLAB and Simulink. Main grid is 230 KV and the distribution network of the microgrid operates at 4.8 KV. It is assumed that the PCC is at node no. 799. Fig. 8 shows PV and wind power data used for the following simulation. Other parameters and adjustments are according to [15]. It is also assumed that the extreme cases can happen where the charging stations are in full operation when the microgrid

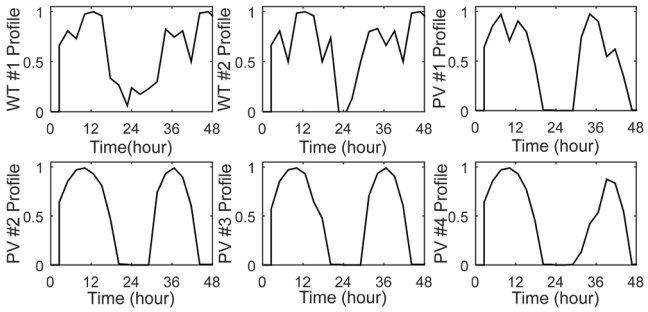

Fig. 8. Assumed wind and PV distributed generation profiles. It should be noted that the EV profiles are according to the stochastic model.

generation is low. Three scenarios are considered in the simulations:

1) The proposed temporal control which includes robust charging control based on the predictive ensembles in the previous section, and instantaneous (real-time) cooperative voltage/power control among DGs and EV stations.
2) Instantaneous cooperative voltage/power control without using predictive ensembles.
3) A base case where no control is applied. In this case, 20% penetration from DGs is assumed.

Fig. 9 shows an operational merit of the proposed stochastic temporal control in comparison with the deterministic instantaneous control and the base case with no control. The differences show that the stochastic optimization makes slight changes to compensate for the upcoming capacity requirements of the network, thus, prevents the increase in the active power requirement to be delivered from the point of common coupling starting at around 18th hour. It should be noted that the energy exchange from the charging stations, Fig. 10, and the reference point for active power exchange through the PCC, equal to 1.6 MW, is chosen to be identical between stochastic/temporal and deterministic/instantaneous cases. In fact, Fig. 10 compares the two control mechanisms on how the same amount of energy would be delivered over the study period.

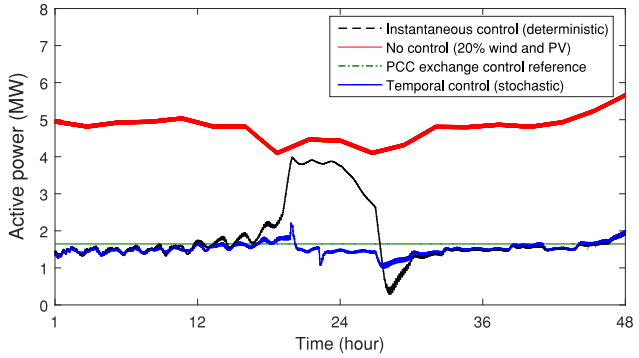

Fig. 9. Active power exchange with the main grid through the PCC.

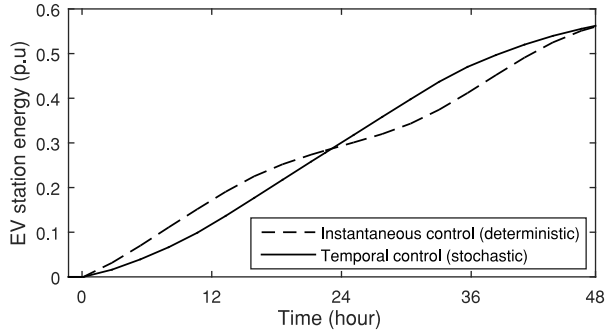

(a)

Fig. 10. Charging stations' energy profile over the study period. Available temporal control and demand response utilizes storage capacity of local energy storage units.

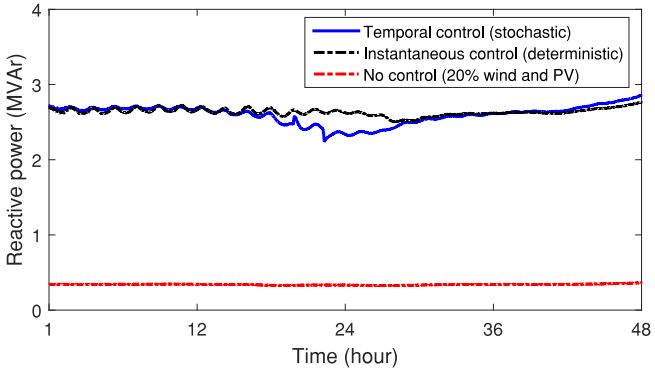

Fig. 11. Reactive power control performance comparison.

The total demand of the station is adjusted by charging control of the local bulk energy storage within the station as well as the V2G operations. Here, V2G operations are kept to a minimum of 12% of the stations capacity. It should be emphasized that the vehicles can be served using the local storage capacity of the charging station. In other words, a reduction in the stations power exchange with the feeder does not necessarily mean a reduction in the number of vehicles served.

The critical performance on the active power exchange could be achieved by applying the analytics-based stochastic constraints in the second-level problem of (13)-(16), with no significant decline in the first-level reactive power and voltage control objectives, i.e., (20). This can be confirmed from

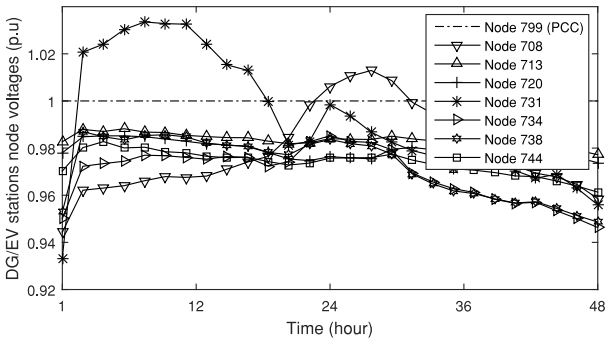

(a)

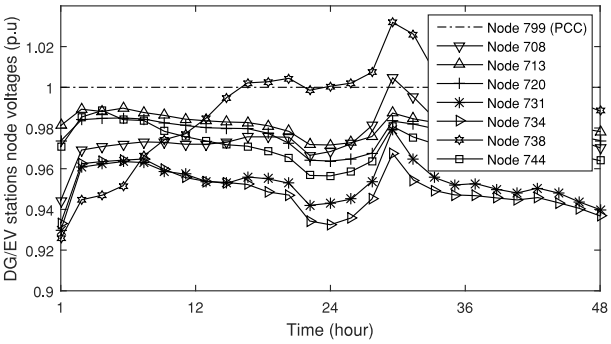

(b)

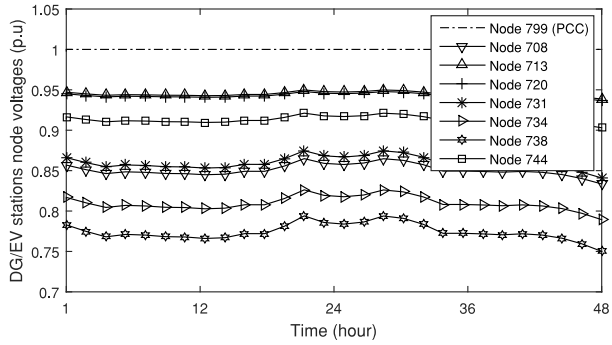

(c)

Fig. 12. Node voltages of the DG and EV charging stations: (a) the proposed temporal control (two-stage), (b) instantaneous control, and (c) no control.

Figs. 11 and 12(a) which show small deviations in reactive power and voltage profiles across the network. Figs. 12(a)–(c) compare three scenarios in terms of their performance to regulate voltage. On one hand, by comparing Figs. 12(a) and 12(b), one can confirm that the additional temporal control stage does not negatively affect the performance of the real-time controls. On the other hand, the significant improvements from the base case with no control (Fig. 12(c)) shows the importance of voltage control for the chosen case study due to the high EV penetration. It should also be noted that a unified grid voltage profile also minimizes the active power loss as shown by [15].

V. Conclusion

This paper proposes a kernel-based predictive model of the EV charging station's capacity. Full distributional characterization and temporal modeling of V2G ensembles

is proposed using a kernel-based copula stochastic process. Temporal interdependence of the projection data and available capacity from charging stations can be captured by the model. Then, by using a stochastic distributed sub-gradient method, power and voltage control of V2G capacity within the network is realized. Optimization and control mechanisms consist of two levels: instantaneous reactive power/voltage control and temporal parameter adjustment and power control. The results show that the obtained solutions can reflect on the system requirements for the upcoming times along with the instantaneous cooperation between distributed resources. In fact, by imposing measures of the most likely ensembles, a distributed sub-gradient method is carried out for cooperative control of the renewable generation and energy storage.

This work introduces basic tools and applications for temporal distributed control within the smart grid, specifically, where the objective is to manage storage, renewable distributed generation, and demand response. Predictive analytics, capable of managing intermittent loads, renewables, rapidly changing weather patterns and other grid conditions, represent the ultimate goal for smart grid capabilities. Within this framework, this research develops high-performance analytics, such as predictive analytics, and ways of employing analytics to improve distributed and cooperative optimization software which proves to be the most significant value-add in the smart grid age, as new network management technologies prove reliable and fundamental.

APPENDIX

PROOF OF THE MULTIVARIATE CONNECTING COPULA EQUATIONS

There can be several solutions to extend the proposed model for multivariate time series data. However, the proposed method in Section II-B that uses a connecting copula reserves the benefits of the univariable case in a multivariable setting [30], [33].

The joint conditional distributions for the multivariable sets of data $\mathbf{X}(t) = \{X_1(t), \ldots, X_N(t)\}$ at time t conditional on the past observations $1, \ldots, t-1$ are used to build the joint unconditional distribution. Hence, the connecting copula is defined as,

$$\Pr\Big(\mathbf{X(t)} < x(t)\Big|\{\mathbf{X(i)} = x(i)\}_{i=1}^{t-1}\Big) \doteq C_b(p_1(t), \ldots, p_N(t)) \tag{25}$$

where, $\mathbf{X}(i) < x(i)$ means $\{X_1(i) < x_1(i), \ldots, X_N(i) < x_N(i)\}$, C_b denotes the connecting copula and

$$\begin{aligned} p_j(t) &= \Pr\Big(X_j(t) < x_j(t)\Big|\big\{X_j(i) = x_j(i)\big\}_{i=1}^{t-1}\Big) \\ &= \frac{\frac{\partial^{t-1}}{\partial x_j(t-1)\cdots\partial x_j(1)} C_j\Big(\big\{F_j\big(x_j(i)\big)\big\}_{i=1}^{t}\Big)}{\frac{\partial^{t-1}}{\partial x_j(t-1)\cdots\partial x_j(1)} C_j\Big(\big\{F_j\big(x_j(i)\big)\big\}_{i=1}^{t-1}\Big)} \\ &= \frac{g_j\Big(\big\{u_j(i)\big\}_{i=1}^{t}\Big)\cdot\prod_{i=1}^{t-1} f_j(x(i))}{c_j\Big(\big\{u_j(i)\big\}_{i=1}^{t-1}\Big)\cdot\prod_{i=1}^{t-1} f_j(x(i))} = \frac{g_j\Big(\big\{u_j(i)\big\}_{i=1}^{t}\Big)}{c_j\Big(\big\{u_j(i)\big\}_{i=1}^{t-1}\Big)} \end{aligned} \tag{26}$$

are the conditional distributions ($j = 1, \ldots, N$). Note that the univariable conditional densities are in terms of the univariable copula C_j that is already learned from the individual data vectors. Also, c_j is the copula density function and g_j is the distribution function calculated by the $(t-1)^{th}$ derivatives of the copula function $C_j(\{F_j(x_j(i))\}_{i=1}^{t})$ with respect to $\{u_j(i)\}_{i=1}^{t-1}$. As used in this paper, $g_j(.)$ for Gaussian copula can be calculated as follows.

$$\begin{aligned} &g_j\{u_i\}_{i=1}^{t}\Big) \\ &= \frac{\partial^{t-1}}{\partial u(t-1)\cdots\partial u(1)} C_j\big(\{u(i)\}_{i=1}^{t}\big) \\ &= \left[\frac{\partial^{t-1}}{\partial v(t-1)\cdots\partial v(1)}\Phi_{(\mathbf{0},\Lambda)}\big(\{u(i)\}_{i=1}^{t}\big)\right]\prod_{i=1}^{t-1}\frac{\partial v(i)}{\partial u(i)} \\ &= \int_{-\infty}^{v(t)}\phi_{(\mathbf{0},\Lambda)}(v(1),\ldots,v(t-1),\gamma)d\gamma\cdot\left[\prod_{i=1}^{t-1}\phi_{(0,1)}v(i)\right]^{-1} \\ &= \left[\prod_{i=1}^{t-1}\phi_{(0,1)}v_i\right]^{-1}\times\int_{-\infty}^{v(t)}\frac{\phi_{(0,\Lambda)}(v(1),\ldots,v(t-1),\gamma)}{\phi_{(\mathbf{0},\mathbf{A})}(v(1),\ldots,v(t-1))} \\ &\qquad\times\phi_{(\mathbf{0},\mathbf{A})}(v(1),\ldots,v(t-1))d\gamma \\ &= \frac{\phi_{(\mathbf{0},\mathbf{A})}(v(1),\ldots,v(t-1))}{\prod_{i=1}^{t-1}\phi_{(0,1)}(v(i))}\int_{-\infty}^{v(t)}\phi_{(\mu,\sigma)}(\gamma)d\gamma \\ &= c_A(u(1),\ldots,u(t-1))\cdot\Phi_{(\mu,\sigma)}(v(t)) \end{aligned} \tag{27}$$

where, $u(i) = F(x(i))$ and $v(i) = \Phi_{(0,1)}^{-1}(u(i))$ and

$$\Lambda = \begin{bmatrix}\mathbf{A} & \mathbf{C}\\ \mathbf{C^T} & b\end{bmatrix} \tag{28}$$

in which, $\{\mathbf{A}_{i,j} = k(x(i), x(j))\}_{i,j=1}^{t-1}$, $b = k(x(t), x(t))$, and $\mathbf{C} = [k(x(t), x(1)), \ldots, k(x(t), x(t-1))]^T$. Furthermore,

$$\mu = \frac{v_t}{b}\mathbf{C}, \tag{29}$$

$$\sigma = \mathbf{A} - \frac{1}{b}\mathbf{C}\mathbf{C}^T. \tag{30}$$

Following on (25), the joint density of current observations, $\mathbf{x_t}$ in terms of all $\{\mathbf{x}(i)\}_{i=1}^{t-1}$ is

$$\Pr\Big(\mathbf{X(t)} < \mathbf{x(t)}\Big|\{\mathbf{X(i)} = \mathbf{x(i)}\}_{i=1}^{t-1}\Big) \tag{31}$$

$$= \frac{\partial^N}{\partial x_1(t)\cdots\partial x_N(t)} C_b(p_1(t), \ldots, p_N(t)) \tag{32}$$

$$= c_b(p_1(t), \ldots, p_N(t))\cdot\prod_{j=1}^{N}\frac{\partial p_j(t)}{\partial x_j(t)} \tag{33}$$

$$= c_b(p_1(t), \ldots, p_N(t))\cdot\prod_{j=1}^{N}\left[\frac{c_j\Big(\big\{u_j(i)\big\}_{i=1}^{t}\Big)}{c_j\Big(\big\{u_j(i)\big\}_{i=1}^{t-1}\Big)}\cdot f_j\big(x_j(t)\big)\right]. \tag{34}$$

Finally, the joint density of the whole multivariable data set, $\{\mathbf{X}(i) = \mathbf{x}(i)\}_{i=1}^{t}$, is given by the product of conditional densities

$$\begin{aligned}\Pr\left(\{\mathbf{X(i)x(i)}\}_{i=1}^{t}\right) &= \Pr\left(\mathbf{X(t)} = \mathbf{x(t)} | \{\mathbf{X(i)} = \mathbf{x(i)}\}_{i=1}^{t-1}\right) \\ &\times \Pr\left(\mathbf{X(t-1)} = \mathbf{x(t-1)} | \{\mathbf{X(i)} = \mathbf{x(i)}\}_{i=1}^{t-2}\right) \\ &\times \Pr\left(\mathbf{X(t-2)} = \mathbf{x(t-2)} | \{\mathbf{X(i)} = \mathbf{x(i)}\}_{i=1}^{t-3}\right) \\ &\times \cdots \times \Pr(\mathbf{X(1)} = \mathbf{x(1)}), \end{aligned} \tag{35}$$

hence,

$$\begin{aligned}\Pr\left(\{\mathbf{X(i)} = \mathbf{x(i)}\}_{i=1}^{t}\right) &= \prod_{\tau=1}^{t}\Bigg[c_b(p_1(\tau), \ldots, p_N(\tau)) \\ &\times \prod_{j=1}^{N}\left(\frac{c_j\left(\{u_j(i)\}_{i=1}^{\tau}\right)}{c_j\left(\{u_j(i)\}_{i=1}^{\tau-1}\right)} \cdot f_j\left(x_j(\tau)\right)\right)\Bigg]\end{aligned} \tag{36}$$

The merit of this model is that the connecting copula can be used to join together different individual copula-based temporal models representing data with completely different dynamics or spatial diversity.

REFERENCES

[1] H. V. Haghi and Z. Qu, "Stochastic distributed optimization of reactive power operations using conditional ensembles of V2G capacity," in *Proc. Amer. Control Conf. (ACC)*, Chicago, IL, USA, Jul. 2015, pp. 3292–3297.

[2] E. L. Karfopoulos and N. D. Hatziargyriou, "Distributed coordination of electric vehicles providing V2G services," *IEEE Trans. Power Syst.*, vol. 31, no. 1, pp. 329–338, Jan. 2016.

[3] A. Y. S. Lam, K.-C. Leung, and V. O. K. Li, "Capacity estimation for vehicle-to-grid frequency regulation services with smart charging mechanism," *IEEE Trans. Smart Grid*, vol. 7, no. 1, pp. 156–166, Jan. 2016.

[4] S. Gao, K. T. Chau, C. Liu, D. Wu, and C. C. Chan, "Integrated energy management of plug-in electric vehicles in power grid with renewables," *IEEE Trans. Veh. Technol.*, vol. 63, no. 7, pp. 3019–3027, Sep. 2014.

[5] Y. Ota *et al.*, "Autonomous distributed V2G (vehicle-to-grid) satisfying scheduled charging," *IEEE Trans. Smart Grid*, vol. 3, no. 1, pp. 559–564, Mar. 2012.

[6] M. Brenna, F. Foiadelli, and M. Longo, "The exploitation of vehicle-to-grid function for power quality improvement in a smart grid," *IEEE Trans. Intell. Transp. Syst.*, vol. 15, no. 5, pp. 2169–2177, Oct. 2014.

[7] M. Falahi, H.-M. Chou, M. Ehsani, L. Xie, and K. L. Butler-Purry, "Potential power quality benefits of electric vehicles," *IEEE Trans. Sustain. Energy*, vol. 4, no. 4, pp. 1016–1023, Oct. 2013.

[8] L. Cheng, Y. Chang, and R. Huang, "Mitigating voltage problem in distribution system with distributed solar generation using electric vehicles," *IEEE Trans. Sustain. Energy*, vol. 6, no. 4, pp. 1475–1484, Oct. 2015.

[9] F. Guo, E. Inoa, W. Choi, and J. Wang, "Study on global optimization and control strategy development for a PHEV charging facility," *IEEE Trans. Veh. Technol.*, vol. 61, no. 6, pp. 2431–2441, Jul. 2012.

[10] S. Hashemi, J. Ostergaard, and G. Yang, "A scenario-based approach for energy storage capacity determination in LV grids with high PV penetration," *IEEE Trans. Smart Grid*, vol. 5, no. 3, pp. 1514–1522, May 2014.

[11] M. Yilmaz and P. T. Krein, "Review of the impact of vehicle-to-grid technologies on distribution systems and utility interfaces," *IEEE Trans. Power Electron.*, vol. 28, no. 12, pp. 5673–5689, Dec. 2013.

[12] E. Sortomme and M. A. El-Sharkawi, "Optimal charging strategies for unidirectional vehicle-to-grid," *IEEE Trans. Smart Grid*, vol. 2, no. 1, pp. 131–138, Mar. 2011.

[13] W. Kempton and J. Tomić, "Vehicle-to-grid power implementation: From stabilizing the grid to supporting large-scale renewable energy," *J. Power Sources*, vol. 144, no. 1, pp. 280–294, 2005.

[14] M. C. Kisacikoglu, B. Ozpineci, and L. M. Tolbert, "EV/PHEV bidirectional charger assessment for V2G reactive power operation," *IEEE Trans. Power Electron.*, vol. 28, no. 12, pp. 5717–5727, Dec. 2013.

[15] A. Maknouninejad and Z. Qu, "Realizing unified microgrid voltage profile and loss minimization: A cooperative distributed optimization and control approach," *IEEE Trans. Smart Grid*, vol. 5, no. 4, pp. 1621–1630, Jul. 2014.

[16] A. Maknouninejad, W. Lin, H. G. Harno, Z. Qu, and M. A. Simaan, "Cooperative control for self-organizing microgrids and game strategies for optimal dispatch of distributed renewable generations," *Energy Syst.*, vol. 3, no. 1, pp. 23–60, 2012.

[17] A. Nedić and D. P. Bertsekas, "Incremental subgradient method for nondifferentiable optimization," *SIAM J. Optim.*, vol. 12, no. 1, pp. 109–138, 2001.

[18] S. S. Ram, A. Nedić, and V. V. Veeravalli, "Incremental stochastic sub-gradient algorithms for convex optimization," *SIAM J. Optim.*, vol. 20, no. 2, pp. 691–717, 2009. [Online]. Available: http://arxiv.org/abs/0806.1092

[19] K. Clement-Nyns, E. Haesen, and J. Driesen, "The impact of charging plug-in hybrid electric vehicles on a residential distribution grid," *IEEE Trans. Power Syst.*, vol. 25, no. 1, pp. 371–380, Feb. 2010.

[20] H. Turker, S. Bacha, D. Chatroux, and A. Hably, "Low-voltage transformer loss-of-life assessments for a high penetration of plug-in hybrid electric vehicles (PHEVs)," *IEEE Trans. Power Del.*, vol. 27, no. 3, pp. 1323–1331, Jul. 2012.

[21] J. C. Gomez and M. M. Morcos, "Impact of EV battery chargers on the power quality of distribution systems," *IEEE Trans. Power Del.*, vol. 18, no. 3, pp. 975–981, Jul. 2003.

[22] W. Kempton and J. Tomić, "Vehicle-to-grid power fundamentals: Calculating capacity and net revenue," *J. Power Source*, vol. 144, no. 1, pp. 268–279, Jun. 2005.

[23] N. Rotering and M. Ilic, "Optimal charge control of plug-in hybrid electric vehicles in deregulated electricity markets," *IEEE Trans. Power Syst.*, vol. 26, no. 3, pp. 1021–1029, Aug. 2011.

[24] R.-C. Leou, C.-L. Su, and C.-N. Lu, "Stochastic analyses of electric vehicle charging impacts on distribution network," *IEEE Trans. Power Syst.*, vol. 29, no. 3, pp. 1055–1063, May 2014.

[25] A. Rautiainen *et al.*, "Statistical charging load modeling of PHEVs in electricity distribution networks using national travel survey data," *IEEE Trans. Smart Grid*, vol. 3, no. 4, pp. 1650–1659, Dec. 2012.

[26] C. Chatfield, "Prediction intervals for time-series forecasting," in *Principles of Forecasting: A Handbook for Practitioners and Researchers*, J. S. Armstrong, Ed. New York, NY, USA: Springer-Verlag, 2001, pp. 475–494.

[27] R. B. Nelsen, *An Introduction to Copulas*. New York, NY, USA: Springer, 2006.

[28] T. Gneiting and M. Katzfuss, "Probabilistic forecasting," *Annu. Rev. Stat. Appl.*, vol. 1, pp. 125–151, Jan. 2014.

[29] A. Lau and P. McSharry, "Approaches for multi-step density forecasts with application to aggregated wind power," *Ann. Appl. Stat.*, vol. 4, no. 3, pp. 1311–1341, 2010.

[30] H. V. Haghi, M. T. Bina, and M. A. Golkar, "Nonlinear modeling of temporal wind power variations," *IEEE Trans. Sustain. Energy*, vol. 4, no. 4, pp. 838–848, Oct. 2013.

[31] Distribution Test Feeders. (Jul. 2015). *IEEE PES Distribution System Analysis Subcommittee's Distribution Test Feeder Working Group*. [Online]. Available: http://ewh.ieee.org/soc/pes/dsacom/testfeeders/

[32] R Core Team, *R: A Language and Environment for Statistical Computing*, R Found. Stat. Comput., Vienna, Austria, 2016.

[33] W. Buntine, M. Grobelnik, D. Mladenic, and J. Shawe-Taylor, Eds., *Machine Learning and Knowledge Discovery in Databases*. Berlin, Germany: Springer-Verlag, 2009.

[34] C. E. Rasmussen and C. K. I. Williams, *Gaussian Processes for Machine Learning*. Cambridge, MA, USA: MIT Press, 2006.

[35] B. Schölkopf and A. J. Smola, *Learning With Kernels*. Cambridge, MA, USA: MIT Press, 2002.

Hamed Valizadeh Haghi, photograph and biography not available at the time of publication.

Zhihua Qu, photograph and biography not available at the time of publication.